6-2018

Theoretical and experimental investigation of forward spatter of blood from a gunshot

P. M. Comiskey
University of Illinois at Chicago

A. L. Yarin
University of Illinois at Chicago

Daniel Attinger
Iowa State University, attinger@iastate.edu

Theoretical and experimental investigation of forward spatter of blood from a gunshot

Abstract
A theoretical model predicting forward blood spatter patterns resulting from a round nose bullet gunshot wound is proposed. The chaotic disintegration of a blood layer located ahead and aside of the bullet is considered in the framework of percolation theory. The size distribution of blood drops is determined, which allows for the prediction of a blood spatter cloud being ejected from the rear side of the target where the bullet exits. Then, droplet trajectories are numerically predicted accounting for gravity and air drag, which is affected by the collective aerodynamic interaction of drops through air. The model predicts the number and area of individual stains, as well as the stain distribution as a function of distance from the region of origin. The theoretical predictions are compared with experimental data acquired in this work from 9 mm Luger copper full metal jacket bullets fired from a handgun. The agreement between the predicted and experimentally measured parameters is found to be good.

Disciplines
Applied Mechanics | Fluid Dynamics | Mechanical Engineering

Comments
This article is published as Comiskey, P. M., A. L. Yarin, and D. Attinger. "Theoretical and experimental investigation of forward spatter of blood from a gunshot." *Physical Review Fluids* 3, no. 6 (2018): 063901. DOI: 10.1103/PhysRevFluids.3.063901. Posted with permission.

Theoretical and experimental investigation of forward spatter of blood from a gunshot

P. M. Comiskey,[1] A. L. Yarin,[1,*] and D. Attinger[2]

[1]*Department of Mechanical and Industrial Engineering, University of Illinois at Chicago, 842 West Taylor Street, Chicago, Illinois 60607-7022, USA*

[2]*Department of Mechanical Engineering, Iowa State University, 2529 Union Drive, Ames, Iowa 60011-1210, USA*

(Received 14 December 2017; published 15 June 2018)

A theoretical model predicting forward blood spatter patterns resulting from a round nose bullet gunshot wound is proposed. The chaotic disintegration of a blood layer located ahead and aside of the bullet is considered in the framework of percolation theory. The size distribution of blood drops is determined, which allows for the prediction of a blood spatter cloud being ejected from the rear side of the target where the bullet exits. Then, droplet trajectories are numerically predicted accounting for gravity and air drag, which is affected by the collective aerodynamic interaction of drops through air. The model predicts the number and area of individual stains, as well as the stain distribution as a function of distance from the region of origin. The theoretical predictions are compared with experimental data acquired in this work from 9 mm Luger copper full metal jacket bullets fired from a handgun. The agreement between the predicted and experimentally measured parameters is found to be good.

DOI: 10.1103/PhysRevFluids.3.063901

I. INTRODUCTION

Blood spatters due to a gunshot are caused by blood ejected from a wound either in the direction of the bullet motion, termed forward spatter, or in the direction opposite to the bullet motion, called backspatter. The forward or backward spatter ejecta correspond to bloodstain patterns on a floor, a wall, or on the persons involved, and they are used by experts of bloodstain pattern analysis (BPA) for the general purpose of crime scene reconstruction [1]. For instance, the aim of BPA is to determine the positions of the victim and perpetrator(s), as well as the sequence and type of events that occurred [2].

Currently, BPA reconstruction of blood drop trajectories relies on several assumptions. For example, a common assumption that has been in use since at least as early as the 1950s [3] is called the straight-line trajectory assumption, and it forms the basis of a class of evaluation techniques known as the method of strings, which is routinely used in software today [4–8]. By assuming that drops travel in straight lines between the wound and the stain location, the reconstruction procedure neglects the effects of air drag and gravity on the trajectories of the blood drops [2]. It is known by forensics experts that the use of straight line trajectories can reduce the reconstruction accuracy, thus the determination of the region of origin, which is the location from which the blood spatter ejecta was issued, can be inaccurate [9,10]. It was reported that the method "overestimates the height of the point of origin and the error associated with this technique is significant (50% on average)" [11]. When gravity and air drag forces are included in ballistic calculations for the reconstruction of

*Author to whom all correspondence should be addressed: ayarin@uic.edu

drop trajectories, the location of origin has been predicted with an approximately four times higher accuracy than using the straight-line trajectory assumption [12].

The physical mechanism of blood drop formation and acceleration in the region of origin in the case of backspatter has recently been discussed and attributed to the Rayleigh-Taylor instability [13,14]. An understanding of the formation of blood drops is an important prerequisite for predicting their trajectories because their initial size, quantity, and corresponding velocities influence the trajectories. Such modeling might allow BPA experts to more accurately reconstruct the events of a crime scene, for example in cases when the type of gun used is unknown.

The physical mechanism of blood spatter generation has so far been studied in detail for backward spatter, but not for forward spatter. These spatter pattern ejecta types are different and may result in quite different spatter patterns [15]. In the latter work, it was revealed that the maximum velocity of forward spattered drops is approximately two times higher than that of their backward spattered counterparts. Moreover, it was found that there are more drops generated in forward spatter and they are grouped in a more compact fashion in flight. These physical facts have several consequences for the development of modeling methods. For instance, the faster velocities may result in drops with larger deformations in flight, which can possibly render the common drag coefficient correlations, such as the Schiller-Naumann or Clift-Gauvin correlations [1,16], inaccurate, or even trigger further atomization events. The effect of drops cooling in flight has been studied before [17] but never in the context of BPA, where the cooling from body temperature to ambient air might affect atomization, spreading, splashing, etc.

There is essentially no scientific literature on the mechanisms of forward spatter pattern formation, to the best of our knowledge, and this could be due to the difficult nature of the problem. It is clear, however, that the damaged tissue ahead of the bullet is the material from which the forward spatter ejecta originates [18]. Understanding the formation of forward blood spatters might help crime scene reconstruction, supplementing information obtained from ballistic reconstruction of bullet trajectories. The latter information is sometimes confusing or complex because bullets can travel long distances without striking an object within the crime scene or might not even be recovered at all. Thus, accurately determining the trajectory of the bullet is not always possible, especially if there are multiple bullets involved throughout a crime scene. It may be a challenge to associate a specific hole or bullet to a given forward spatter pattern. Combining the reconstruction of the bullet and blood drop trajectories may yield the location of the victim. In addition, in cases involving multiple shooters, forward spatter patterns in conjunction with bullet comparisons may help identify which gun/shooter fired the fatal shot. Lastly, muzzle gases may have less of an effect on forward spatter pattern distribution than on backward spatter.

In the present work, the forward spatter pattern and the formation of blood drops which created that pattern are linked through physics-based modeling. In contrast with the Rayleigh-Taylor instability mechanism of blood drop formation previously proposed for back spatter due to a gunshot [13,14], chaotic disintegration characteristic of debris formation in terminal ballistics [16,19,20], which encompasses multiple instability cycles in the framework of percolation theory, is in focus. That means that in contrast with the back spatter attributed to a straightforward Rayleigh-Taylor instability of blood at first contact with the bullet, forward spatter follows the penetration of the bullet through a body, which is accompanied by a cascade of multiple instabilities and rupture phenomena, characteristic of the problems of terminal ballistics. The complexity of such situations is adequately tackled by percolation theory [19,20], and as such this approach is adopted in the present work. The aim is to develop a model of forward blood spatter that is to be verified experimentally. In relation to liquids subjected to high-speed impacts, such disintegration is called a fracture or "cavitation" [21–24]. The resultant model allows for the prediction of drop sizes, the magnitude and direction of their initial velocities, as well as accounts for gravity and air drag with collective effects that determine drop motion, final locations, stain areas, impact velocities and angles, and any other parameter of interest. Section II describes the experiments conducted in the present work, and Sec. III presents the theoretical approach. Results are discussed and compared with the experimental data in Sec. IV, and finally conclusions are drawn in Sec. V.

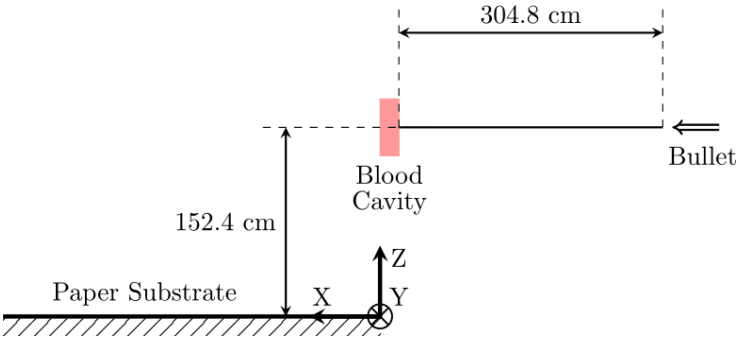

FIG. 1. Schematic of the forward spatter experimental setup. The muzzle of the gun was located 304.8 cm away from the target, which was impacted by the bullet normally at 152.4 cm above the ground. The bullet completely perforated the target to produce a forward spatter pattern on the horizontally laid butcher paper substrate behind the target. The target thickness was 5 mm and the radius of the bullet was 4.5 mm.

II. EXPERIMENT

The experimental forward spatter patterns were created at the Kansas City Police Department Crime Lab in Kansas City, MO. In an attempt to construct a reproducible blood source, a closed blood-filled reservoir was prepared as follows. A $4 \times 4\,\mathrm{cm}^2$ section of paper was peeled back from one side of foam board (Elmer's, USA). Approximately 5 mm of exposed foam in a central $2 \times 2\,\mathrm{cm}^2$ section was then removed; the cavity was filled with 2 mL of whole human blood containing EDTA anticoagulant from a single individual. Clear packaging tape was utilized to affix the paper back over the blood-filled section. The blood was allowed to cool to 20–22 °C and prior to shooting, the foam board was gently agitated to ensure homogenous displacement and limit coagulation within each cavity.

Each cavity containing 2 mL of blood was shot only once with an American Eagle (Federal Premium, USA) 9 mm Luger bullet with a full metal copper jacket fired from a 9 mm Glock model 19 (Glock, Inc., USA) semiautomatic pistol mounted in a remote firing device. Per the manufacturer, each bullet weighed 7.45 g and was 9 mm in diameter by 19 mm in length. The muzzle was located 304.8 cm (10 ft) from the front side of the target and was aligned to fire a bullet for impact normally at 152.4 cm (5 ft) above the ground (cf. Fig. 1). The average muzzle velocity of the bullet was found to be 351 m/s as determined from five trials via a chronograph (Competitive Edge Dynamics Model M2).

The blood spatter was produced on a butcher paper substrate strip ($0.41 \times 4\,\mathrm{m}^2$) located on the floor behind the target. The substrate was then digitally scanned at 600 dpi and analyzed for the number of stains and their areas as a function of the distance traveled from the rear side of the target. The parameters of interest were binned from 25–400 cm in 25-cm-wide strips.

Note that the reported experimental results are the combination of the number of stains and their average areas over the five conducted trials. Namely, the number of stains were added for the five experiments, and then, the stain area was averaged stripwise. The theoretical predictions were organized accordingly. The results were reported in this way to minimize the effect of any minor irreproducibility such as the bullet impacting the target off-center or arriving non-normal to the surface. Moreover, if there are multiple gunshot wounds, it can be difficult for BPA experts to attribute which bloodstain occurred as a result of a specific gunshot wound. Therefore, the total number of stains is a result of interest. Their respective stain areas were averaged over all five replicates to get an impression of the possible distribution of stain sizes.

III. THEORETICAL

The formation of blood spatter due to a bullet impact is a short-term event in which the viscous forces are negligibly small compared to the inertial ones because the Reynolds number is of the order

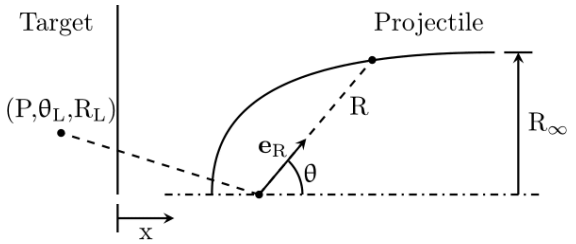

FIG. 2. Schematic of the coordinates and variables used in the theoretical model.

of 10^7 [13]. Blood spatter formation in forward spatter involves a cascade of instability phenomena, and in this sense is seemingly more involved than in the case of backward spatter, where at least the first group of spattered drops is formed due to the Rayleigh-Taylor instability associated with acceleration of denser blood toward lighter surrounding air [13,14]. It was also found recently that the maximum velocity of forward spattered drops is approximately two times higher than that of backwards spattered ones partially due to the entrainment effect of the bullet traveling in the same direction as the forward blood spatter [15].

Given the above facts, an appropriate atomization model might be one of chaotic disintegration. Such models were developed previously in the framework of percolation theory to predict the debris formation in terminal ballistics, as detailed in Sec. III A [16,19,20]. After atomization, the drops move through air and experience gravity and air drag forces, with the latter being diminished for the inner drops in the cloud due to collective effects associated with the aerodynamic drop-drop interaction [13–15,25,26]. At rates of strain as high as those characteristic of forward spatter, the viscoelasticity of blood [27] can significantly reduce drop ejection velocities, and thus should be accounted for.

The framework of the theoretical model is built around percolation theory. First, the probability field within the target is established, and the fragmented sections are determined under the condition that the probability of a site being occupied by liquid $P < P^*$, with the latter being the critical probability value (a fully geometrical parameter known from percolation theory). This is described in Sec. III A. Then in Sec. III B, the fragmented section is discretized into bins that have the predicted initial velocities, inclination angles, and characteristic sizes. The effect of blood viscoelasticity creates a web of blood that decelerates and reconnects droplets forming a strongly interconnected web and is described in Sec. III C. Finally, the trajectories of the blood droplet spray are predicted following our recent work [13].

A. Chaotic disintegration of a liquid

The problem of forward spatter formation is posed similarly to the formation of debris due to bullet impact and is shown schematically in Fig. 2 [16,20]. The flow field within the blood-impregnated target is potential. The bullet is assumed to be shaped like an ovoid of Rankine, which is equivalent to parallel flow superimposed on a single source. The surface of the axially symmetric ovoid of Rankine in spherical coordinates with the source at the coordinate system origin is given by [28] as

$$R = \frac{R_\infty}{2\sin(\theta/2)}, \tag{1}$$

where R is the radial coordinate, θ is the zenith angle reckoned from the parallel flow direction, with $\theta = \pi$ corresponding to the tip of the bullet, and R_∞ being the cross-sectional radius of the ovoid of Rankine at infinity. The potential flow field generated in the target by the penetrating ovoid of Rankine and resulting from its disjoining action possesses the velocity vector

$$\mathbf{v}_T = -\frac{\dot{x}R_\infty^2}{4R^2}\mathbf{e}_R, \tag{2}$$

where $\dot{x}$ is the velocity of the ovoid of Rankine, and $\mathbf{e}_R$ is the unit vector in the radial direction. Note that the coordinate x is reckoned from the front surface of the target outward, which means that $x \leqslant 0$ is within the target.

The target undergoes fragmentation into drops due to the angular stretching imposed by the penetrating axisymmetric bullet. When the kinetic energy of deformation becomes equal to the surface energy of a liquid element under consideration, the fragmentation process cannot be sustained anymore. Therefore, the smallest (indivisible) drop size, a_0, is determined by the equality [19]

$$\tfrac{1}{2}\rho a_0^3(\dot{\varepsilon}a_0)^2 = \gamma a_0^2, \tag{3}$$

where ρ is the density of the liquid target, 1060 kg/m^3, γ is the surface tension of blood, 60.45 mN/m [27], and $\dot{\varepsilon}$ is the local rate of strain. The rate of strain in the target is of the order of

$$\dot{\varepsilon} \sim \frac{|\dot{x}|R_\infty^2}{R^3}, \tag{4}$$

which shows that the azimuthal stretching process fades as $1/\mathrm{R}^3$. Equations (3) and (4) yield

$$a_0 \sim \left(\frac{\gamma}{\rho\dot{\varepsilon}^2}\right)^{1/3} = R_\infty \alpha^{1/3}\overline{R}^2, \tag{5}$$

$$V_0 = \frac{4}{3}\pi a_0^3 = \frac{4}{3}\pi R_\infty^3 \alpha \overline{R}^6, \tag{6}$$

where V_0 is the volume of the smallest drop, $\bar{R} = R/R_\infty$, and

$$\alpha = \frac{\gamma}{\rho|\dot{x}|^2 R_\infty}. \tag{7}$$

Note that Eq. (5) is essentially an order-of-magnitude estimate, where the factor of the order of 1 is immaterial [19,20].

As previously mentioned, the local elements of the target are fragmented due to angular stretching. This causes a random lacunae growth identical to multiple observations of liquid fracture ("cavitation") caused by a high-speed impact (e.g., bullet) or explosion [21–24]. To account for the random nature of such a fragmentation process, percolation theory can be applied [16,19,29,30]. It should be emphasized that percolation theory is essentially a purely geometric description, which underlies the essence of multiple physical phenomena, and thus is applicable to any medium (liquid or solid). A volume of an envelope encompassing an element of a target that is undergoing fragmentation, dV_T, can be estimated as

$$dV_T = dV_{T0}\left(1 + \int_0^t \frac{|\dot{x}|R_\infty^2}{R^3}dt\right)^3, \tag{8}$$

where dV_{T0} is the initial element volume of that element. The corresponding probability that an elementary particle of the size a_0 is within an elementary site inside dV_T is

$$P(t) = \frac{dV_{T0}}{dV_{T0}\left(1 + \int_0^t \frac{|\dot{x}|R_\infty^2}{R^3}dt\right)^3}. \tag{9}$$

As $t \to \infty$, the probability that a particle of size a_0 occupies an elementary site within dV_T decreases, since the angular stretching (and thus lacunae growth) continues. Therefore, there exists a certain time moment at which the probability becomes subcritical and thus small enough for an infinite cluster of the occupied elementary sites to cease existing. The critical probability value may be taken as $P^* = 0.311$ for three-dimensional percolation [19,20,29,30]. In the subcritical case only finite clusters can exist, which corresponds to drops of different sizes comprised of a different number of elementary droplets of size a_0.

In the framework of the Lagrangian description of the target deformation in the present axisymmetric case, the probability field within the target $P(R,\theta,t)$ can be found. The initial radial and angular positions of a material element are denoted as θ_0 and R_0, whereas the current positions of this material element are denoted as θ_L and R_L. Then, the following set of ordinary differential equations describes the evolution of the probability field and the current coordinates of the material element in time:

$$\frac{d}{dt}(P^{-1/3}) = \frac{|\dot{x}|R_\infty^2}{R_L^3}, \tag{10}$$

$$\frac{dR_L}{dt} = \mathbf{v}_T \cdot \mathbf{e}_R + |\dot{x}|\cos\theta_L, \tag{11}$$

$$\frac{d\theta_L}{dt} = \frac{1}{R_L}(\mathbf{v}_T \cdot \mathbf{e}_\theta - |\dot{x}|\sin\theta_L), \tag{12}$$

where Eq. (10) is obtained from Eq. (9) by differentiation in time.

Given that $|\dot{x}|dt = d|x|$ (cf. Fig. 2 having in mind that $x < 0$ and $\dot{x} < 0$), Eqs. (10)–(12) take the following dimensionless form:

$$\frac{d}{d|\bar{x}|}(P^{-1/3}) = \frac{1}{\bar{R}_L^3}, \tag{13}$$

$$\frac{d\bar{R}_L}{d|\bar{x}|} = \frac{1}{4\bar{R}_L^2} + \cos\theta_L, \tag{14}$$

$$\frac{d\theta_L}{d|\bar{x}|} = -\frac{1}{\bar{R}_L}\sin\theta_L. \tag{15}$$

Here R_L and x are rendered dimensionless by R_∞. Equations (13)–(15) are solved using the following initial conditions:

$$|\bar{x}| = 0 : P = 1, \quad R_L = R_0, \quad \theta_L = \theta_0. \tag{16}$$

The analytical solutions of Eqs. (13) and (14) read [16,20]

$$\bar{R}_L = \left(\frac{\cos\theta_L - \cos\theta_0 + 2\bar{R}_0^2\sin^2\theta_0}{2\sin^2\theta_L}\right)^{1/2}, \tag{17}$$

$$P = \left\{1 + 2\ln\left|\frac{\bar{R}_L^2\sin^2\theta_L}{\bar{R}_0^2\sin^2\theta_0}\right|\right\}^{-3}, \tag{18}$$

where $\bar{R}_0 = R_0/R_\infty$. The equation for the current angular position of the material element, Eq. (15), however, must be simultaneously numerically integrated for different material elements of the target corresponding to different values of R_0 and θ_0, as

$$\frac{d\theta_L}{d|\bar{x}|} = -\frac{\sqrt{2}\sin^2\theta_L}{\left(\cos\theta_L - \cos\theta_0 + 2\bar{R}_0^2\sin^2\theta_0\right)^{1/2}}. \tag{19}$$

Note that Eqs. (17) and (18) are singular at $\theta_L = \theta_0 = \pi$. The singularity in the limit $\theta \to \pi$ is removed by introducing $\delta_\theta = \pi - \theta \ll 1$ as $\theta \to \pi$. Then, Eqs. (13)–(15) reduce to the following

equations:

$$\frac{d}{d|\bar{x}|}(P^{-1/3}) = \frac{1}{\bar{R}_L^3}, \tag{20}$$

$$\frac{d\bar{R}_L}{d|\bar{x}|} = \frac{1}{4\bar{R}_L^2} - 1 + O\left(\delta_\theta^2\right), \tag{21}$$

$$\frac{d\delta_\theta}{d|\bar{x}|} = \frac{\delta_\theta}{\bar{R}_L} + O\left(\delta_\theta^2\right). \tag{22}$$

The analytical solutions of the latter three equations read [16,20]

$$P = \left\{1 + 2\ln\left|\frac{\bar{R}_L^2}{4\bar{R}_L^2 - 1}\right| - 2\ln\left|\frac{\bar{R}_0^2}{4\bar{R}_0^2 - 1}\right|\right\}^{-3}, \tag{23}$$

$$4\bar{R}_0 - \ln\left|\frac{2\bar{R}_0 + 1}{2\bar{R}_0 - 1}\right| = 4|\bar{x}| + 4\bar{R}_L - \ln\left|\frac{2\bar{R}_L + 1}{2\bar{R}_L - 1}\right|, \tag{24}$$

$$\delta_{\theta L} = \delta_{\theta 0}\left(\frac{4\bar{R}_0^2 - 1}{4\bar{R}_L^2 - 1}\right)^{1/2}, \tag{25}$$

where $\delta_{\theta L} = \pi - \theta_L$ and $\delta_{\theta 0} = \pi - \theta_0$.

The probability that a material element of elementary size a_0 occupies a site in proximity to the bullet axis is thus found and its current position along that axis is determined by Eq. (24). However, at the bullet tip, Eqs. (23) and (24) become singular since there, $\bar{R}_L = \bar{R}_0 = 1/2$, which means that the asymptotic behavior at this point must also be further explored. Defining $\delta_R \ll 1$, Eq. (23) for $P = P(R_L)$ and Eq. (24) for $R_L = R_L(x)$ can be linearized about the tip point, $\delta_R = 0$, which yields

$$P = \{1 + 8|x|\}^{-3} + \frac{24(1 - e^{-4|x|})}{(1 + 8|x|)^4}\delta_R + O\left(\delta_R^2\right). \tag{26}$$

The probability that an elementary droplet of size a_0 occupies any site inside the target domain undergoing fragmentation at time t after impact is thus found.

It should be emphasized that an analytical solution for the magnitude of the coordinate of the tip of the fractured zone in the target $|\bar{x}|^*$ at time t^* reckoned from the front surface of the target can be found using Eqs. (23) and (24) as

$$|\bar{x}|^* = \bar{H} + \frac{1}{2} - \bar{R}^* + \frac{1}{4}\left(\ln\left|\frac{2\bar{R}^* + 1}{2\bar{R}^* - 1}\right| - \ln\left|1 + \frac{1}{\bar{H}}\right|\right), \tag{27}$$

where

$$\bar{R}^* = \left(\frac{Q}{4Q - 1}\right)^{1/2}, \tag{28}$$

$$Q = \exp\left[\ln\left|\frac{(\bar{H} + 1/2)^2}{4(\bar{H} + 1/2)^2 - 1}\right| + \frac{(P^*)^{-1/3} - 1}{2}\right], \tag{29}$$

which uses the fact that $\bar{R}_0 = \bar{H} + 1/2$ with $\bar{H} = H/R_\infty$, and H is the target thickness.

To determine the distribution of mass and number of drops (finite clusters) within a volume element in the fractured zone, dV_T, percolation theory is applied. If s is the number of elementary indivisible droplets of size a_0 in a fragment (a finite cluster) emerging from the target ($s \geqslant 1$), the

volume and mass of the fragment can be found using a_0 from Eq. (5) as

$$V = \tfrac{4}{3}\pi R_\infty^3 \alpha \bar{R}^6 s, \tag{30}$$

$$m = \tfrac{4}{3}\pi \rho R_\infty^3 \alpha \bar{R}^6 s. \tag{31}$$

The probability density function corresponding to a cluster of s elementary indivisible droplets of size a_0 is known from percolation theory [19,20,29,30] as

$$w_s = K s^{-\tau+1} \exp(-b s^\zeta), \tag{32}$$

where τ and ζ are known constants determined by the space dimensionality (here we are dealing with a three-dimensional case), b depends on the spatial location within the target, and K is a normalization parameter,

$$K = \frac{1}{\int_1^\infty s^{-\tau+1} \exp(-b s^\zeta) ds}. \tag{33}$$

Using Eqs. (30)–(33), the total number of fragments of mass m_f in the fractured zone of the target, dN, in dV_T is found as

$$dN(m_f) = \frac{3 dV_T K}{4\pi R_\infty^3 \alpha \bar{R}^6} \int_1^{s_f} s^{-\tau} \exp(-b s^\zeta) ds, \tag{34}$$

$$s_f(m_f, \bar{R}) = \max\left[1, \frac{3 m_f}{4\pi \alpha \rho R_\infty^3 \bar{R}^6}\right]. \tag{35}$$

The upper limit of the integration in Eq. (34) is s_f, given by Eq. (35), which is the number of elementary indivisible droplets of size a_0 in the fragment of mass m_f. The total mass of the fractured target corresponding to the fragments beginning from the indivisible elementary one of size a_0 to the one of mass m_f is given by

$$dM(m_f) = \rho dV_T K \int_1^{s_f} s^{-\tau+1} \exp(-b s^\zeta) ds. \tag{36}$$

Accordingly, the total number of fragments (finite clusters, drops) and mass in the fractured zone of the target are equal to

$$N(m_f) = \int_{V_T} dN(m_f), \tag{37}$$

$$M(m_f) = \int_{V_T} dM(m_f), \tag{38}$$

respectively.

Evaluating these integrals using the standard parameter values and the expression familiar in percolation theory [29,30], namely $\tau = 3/2$, $b = 20.84|P^* - P|^{1/\sigma}$, $\sigma = 0.45$, and $\zeta = 1$, results in

$$N(m_f) = -\frac{3\rho|\dot{x}|^2}{2\pi\gamma R_\infty^2} \int_{V_T} \frac{K}{\bar{R}^6} \Big\{ \sqrt{b\pi} [\mathrm{erf}(\sqrt{b s_f}) - \mathrm{erf}(\sqrt{b})] + \exp(-b s_f) s_f^{-1/2} - \exp(-b) \Big\} dV_T, \tag{39}$$

$$M(m_f) = \rho \int_{V_T} \frac{\mathrm{erf}(\sqrt{b s_f}) - \mathrm{erf}(\sqrt{b})}{\mathrm{erfc}(\sqrt{b})} dV_T, \tag{40}$$

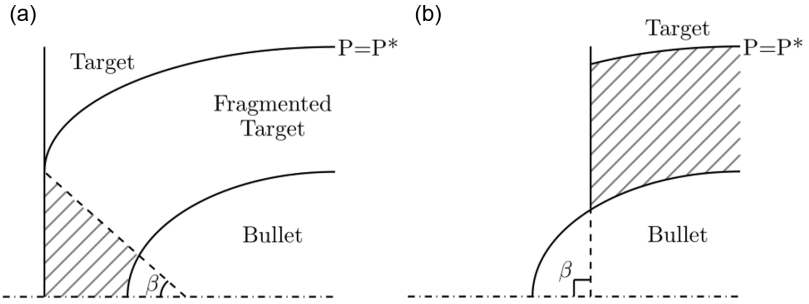

FIG. 3. Target discretization types from the bullet as it travels from the right to the left. The gray cross-hatched section represents the portion of the target in which droplets form and are ejected from the target. (a) Section of the target where V_T is approximated as a cone, and (b) where V_T is approximated as a cylinder.

where the normalization parameter becomes

$$K = \left(\frac{b}{\pi}\right)^{1/2} \frac{1}{\operatorname{erfc}(\sqrt{b})}. \tag{41}$$

Equations (39) and (40) are numerically integrated over the entire fractured volume, V_T, which exists in the target only when $P < P^*$. Directly in front of the leading edge of the bullet, V_T is encompassed by a conelike domain whose apex is at the location of the source generating the ovoid of Rankine (cf. Fig. 3). The boundaries of this domain are fully determined by the critical percolation value P^*. The semiangle of the cone, β, changes as the bullet approaches the rear surface of the target, and at a time instance of $t > t^*$, the fractured zone reaches the rear side of the target and the fragment cone is ejected. Between the time intervals from t (where $t > t^*$) to $t + \Delta t$, a new, hollow fragmented cone emerges as a result of the continuous bullet motion whose volume is found as ΔV_T. Eventually, this volume ΔV_T also leaves the target and the process repeats until $\beta \geqslant \pi/2$ because at that point, the cone approximation of the fractured domain is not valid anymore and is replaced by the cylindrical one. This process continues until the bullet can freely leave the target without any further fragmentation.

B. Drop trajectories

Discretized ringlike slices of the fractured target volume, V_T, are termed bins and denoted by i. The number of drops and their respective masses for each bin are found using Eqs. (39) and (40). These drops are ejected from the target with velocity magnitude $u_i|_{\text{initial}}$ determined by Eq. (2) as

$$u_i|_{\text{intial}} = \dot{x}\sqrt{\frac{R_\infty^4}{16R^4} + 1 - \frac{R_\infty^2}{2R^2}\cos\theta} \tag{42}$$

at the initial inclination angle, φ, which is found as

$$\varphi = \cos^{-1}\left[\left(2 - \frac{R_\infty^2}{2R^2}\cos\theta\right)\left(2\sqrt{\frac{R_\infty^4}{16R^4} + 1 - \frac{R_\infty^2}{2R^2}\cos\theta}\right)^{-1}\right]. \tag{43}$$

Each drop in the ejected bins has a characteristic size, $l_{*,i}$, calculated as

$$l_{*,i} = \left[\frac{6(M_i/N_i)}{\pi\rho}\right]^{1/3}. \tag{44}$$

Each bin is considered as a blood drop spray that entrains air due to the turbulent eddy viscosity, thus forming a two-phase interpenetrating continuum [25,26]. The resultant trajectory equations are

described in detail in our previous work [13]. It should be emphasized that the equation for the coefficient of drag used in the present work is the Schiller-Naumann formula [16]

$$C_{D,i} = \frac{24}{\mathrm{Re}_i}\left(1 + 0.15\mathrm{Re}_i^{0.687}\right), \tag{45}$$

where Re_i is the Reynolds number for each bin. The current results belong to the range of validity of this widely used correlation. Another option would be the empirical formula for the drag coefficient discussed in [1].

C. Effect of blood elasticity on forward blood spatter

Consider a single drop of a characteristic size $l_{*,i}$, disconnecting from the target at a velocity $u_i|_{\mathrm{initial}}$. Since blood is a complex, non-Newtonian fluid that exhibits viscoelastic behavior [27,31–33], elastic stresses can build up in the rapidly stretching drop tails. Such tails are inevitably formed during the ejection of a viscoelastic fluid at a sufficiently high initial velocity of the drops in a short-time detachment process, i.e., when the Deborah number, De, is $\mathrm{De} \gg 1$ [19,27,34]. Here, the Deborah number is the ratio of the blood elastic relaxation time, λ, to the characteristic time of the tail detachment process $t_{\mathrm{det},i}$, i.e., $\mathrm{De} = \lambda/t_{\mathrm{det},i}$. Note that in non-Newtonian fluid mechanics, flows with $\mathrm{De} \gg 1$ are called strong flows. Drop tails are inevitably formed as drops separate from ligaments, films, or fully three-dimensional liquid bodies. Tail formation in viscoelastic fluids from strong elongational flows is due to significant elastic stresses. This effect was explored in detail, for example, in [35]. A similar flow scenario is present as in the current case of projectile-induced flow. It should be emphasized that at $\mathrm{De} \gg 1$, the rheological behavior of any material essentially resembles an elastic solid. As a result, high-speed collisions with all liquids including blood cause a shock wave front to propagate followed by a rarefaction wave, which induces cavitation and solidlike brittle fracture. These spallation (fragmentation) phenomena have been experimentally observed to occur in both Newtonian viscous and in practically inviscid and non-Newtonian viscoelastic liquids [21–24,36], where, for example, the brittle fracture of a liquid jet was demonstrated starting from the impact velocity as low as 23 m/s [21]. Because the impact velocity of the bullet in the current case, $|\dot{x}| = 351$ m/s, is much higher than this threshold, it is assumed that the blood droplet tails undergo brittle fracture.

The buildup of the elastic stresses in the drop tail, evident from the estimates [27] and substantiated by detailed calculations in Sec. IV, can decelerate the drop detachment process and diminish its initial ejection velocity. It should be emphasized that in the previous models of backward spatter [13,14], blood viscoelasticity was not accounted for because the drop detachment velocities there were significantly lower than in the present case of forward spatter. For example, in a previous experiment where both forward and backward spatter were observed, at 0.45 ms after bullet impact, droplet velocity in the forward spatter case was 40 m/s, whereas for backward spatter it was only 8 m/s [15], with the former being higher than the threshold velocity of brittle fracture of 23 m/s [21], whereas the latter was lower. Accordingly, in the present case, consider a drop tail of size L_i, which still spans the detaching drop and the main body of the target. Its evolution is determined by the following kinematic equation and the momentum balance, respectively:

$$\frac{dL_i}{dt} = u_i, \tag{46}$$

$$\rho\frac{4\pi}{3}\left(\frac{l_{*,i}}{2}\right)^3\frac{du_i}{dt} = -\pi\left(\frac{l_{*,i}}{2}\right)^2 3G\varepsilon_{xx}, \tag{47}$$

where, u_i is the current drop velocity, G is the elastic shear modulus, and $\varepsilon_{xx} = (L_i - l_{*,i})/l_{*,i}$, is the tail strain.

In the momentum balance of the drop, subjected to a resistive elastic force acting on it from the stretching tail as described by Eq. (47), a relatively small tail stretching occurs below $L_i \approx l_{*,i}$, and

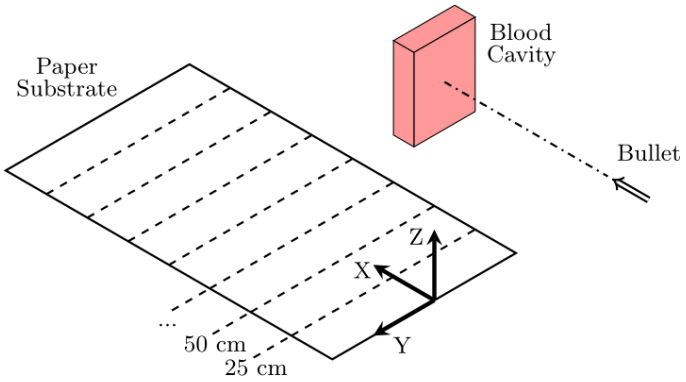

FIG. 4. Schematic of the discretization of the paper substrate. The dashed lines are where the locations of the data points, both theoretical and experimental, are accounted for.

before the fracture would happen, and thus blood elasticity is described using Hooke's law [33]. Note that $G = E/3$, where E is Young's modulus of blood. The latter can be evaluated using the speed of sound in blood, $c = 1570\,\mathrm{m/s}$ [37], and its density, which yields $E = 2.6\,\mathrm{GPa}$.

Equations (46) and (47) yield

$$u_i = u_i|_{\text{initial}} \cos(t_i/T_i), \quad T_i = \left(\frac{2}{3}\frac{\rho l_{*,i}^2}{E}\right)^{1/2}. \tag{48}$$

Droplet detachment time $t_i = t_{\text{det},i}$, which is obviously less than T_i, increases with its size $l_{*,i}$ and an appropriate correlation between $t_{\text{det},i}$ and $l_{*,i}$ is discussed in Sec. IV. It should be emphasized that u_i predicted by Eq. (48) is used as the initial velocity in the simulations of drop trajectories.

IV. RESULTS AND DISCUSSION

At the onset of the bullet penetrating the target, a nearly instantaneous spray is formed that contains many small droplets traveling at a high initial velocity [15]. The theoretical model described in Sec. III predicts that these small droplets form in the target directly ahead of the bullet. These small droplets are rapidly decelerated by air drag and fall down very close to the target. Moreover, high-speed videos of bullet penetration phenomena show that the majority of the resultant blood drop spray stems from the area surrounding the bullet [15] and thus droplets issued from the cross-hatched domain in Fig. 3(a) are disregarded. On the other hand, bigger drops formed and issued from the "cylindrical" cross-hatched domain shown in Fig. 2(b) were fully accounted for and their trajectories tracked. This cylindrical domain was discretized into 20 ringlike slices (bins) spanning the length of the target, as shown in Fig. 4.

To compare the experimental data to the theoretical results, several governing parameters must be specified. Namely, the velocity of the bullet, $\dot{x} = 351\,\mathrm{m/s}$ was used in the simulations, as well as the height at which the bullet impacted the target, $H_0 = 152.4\,\mathrm{cm}$. Since the theoretical model implies the bullet is shaped like an ovoid of Rankine, the latter was fitted to the real bullet shape. Although close, the present bullet was not a perfect ovoid of Rankine. It is unphysical to have the ovoid of Rankine bullet in the numerical simulation to extend past the surface of the actual bullet since the tip shape practically completely determines the flow field in blood, which is substantiated by multiple well-established phenomena in the field of terminal ballistics [38] and is a fundamental assumption in such models as the cavity expansion model developed there. A very good agreement of the shape of the ovoid of Rankine can be achieved with the leading part of the real bullet (Fig. 5). This, however, reached only 3/4 of the real bullet radius (i.e., $R_\infty = 3.375\,\mathrm{mm}$) at "infinity," which was considered to be tolerable. The thickness of the target was set to be equal to R_∞ and the droplet bins issued from

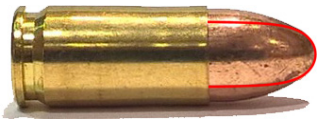

FIG. 5. A 9 mm Luger copper full metal jacket bullet and cartridge casing used in the experiment with the ovoid of Rankine shown by the line superimposed on its leading edge.

only over the top and below the bottom of the bullet (at the azimuthal angles $\phi = 90^\circ$ and 270°; cf. [13]) were tracked numerically. This was motivated by the fact that the experiment was designed in such a way that only a strip of paper directly under the trajectory of the bullet was used to acquire the data.

The configuration of the fragmented "cylindrical" volume (cf. Fig. 3) of the target was predicted at $t = 0.02$ ms after the bullet impact using Eqs. (17) and (19). This means that each slice (bin) in this fragmented volume is fully fragmented accordingly in multiple droplets. The mass and number of droplets issued from each bin was predicted using Eqs. (39) and (40). The initial velocities and inclination angles of the droplets of each bin were predicted by Eqs. (42) and (43) with characteristic sizes calculated by Eq. (44). It should be emphasized that the droplets originating from the bins that are closer to the rear surface of the target move forward slower than the ones originating from the other side. Immediately following the moment of fracture, in a very dense cloud of droplets, such a velocity distribution inevitably causes chaotic multiple drop-drop collisions. Moreover, the following three circumstances should be mentioned. (i) The fragmentation of a target due to a bullet impact is a large-scale phenomenon, albeit the volume of material that actually leaves the target is quite small. An example of this is seen in the seminal images photographed by Harold Edgerton [39]. In an image of a 0.30 caliber bullet impacting a sheet of plexiglass, one can see that there are small fragments leaving the target in the direction of the bullet motion (the forward "spatter") only in the very near vicinity of the bullet impact point. On the other hand, there is a fractured zone that is massive in comparison to the material that actually leaves the target. (ii) The case of the forward spattering of blood due to a gunshot is not dissimilar to the bullet impact on a plexiglass pane due to the fact that at high values of the Deborah number characteristic of bullet impact, blood undergoes brittle fracture, as discussed in Sec. III C. A rough estimate can be done of the volume of blood that is splashed forward, using the high-speed videos of blood spatter due to a gunshot, which were taken by the Midwest Forensic Resource Center [40] and analyzed in [15]. From experiment 7Aa1 in [15], which closely resembles the one here, one estimates that the target looks to be filled with $\sim$10 mL of blood and that only 0.33 cm^3 of blood was splashed (taking the average sizes and estimating the number of droplets splashed), which means that only about 3.3% of blood was actually splashed. It should be emphasized, however, that this is a rough "higher" value, and in some cases it can be much lower. Using the exact number of droplets and average area from [15], for instance, shows that in experiment 7Aa1 [15], the percentage of droplets that leave the target becomes 0.01%. (iii) An additional factor preventing detachment of multiple droplets from the bulk is the formation of long tails that are stabilized by the elastic forces and do not break up (the situation discussed in Sec. III C) and illustrated by the images of disintegrating jets of dilute polymer solutions in [35]. Summarizing, one can state that in any case, the volume of material that escapes the target is extremely small when compared to the volume of the entire fractured part of the target. As a result, it is assumed that 5% of the fractured target results in droplets that form the forward spatter spray.

The relaxation time of swine blood (which shares similarities with human blood [41]) is about $\lambda = 15$ ms [27], bullet penetration happens on the scale of 10^{-5} s, and the fracture process of the blood drop tail is on the order of microseconds, as Eq. (48) reveals given the known input parameters. The droplet tail detachment time is naturally an increasing function of the droplet size, $l_{*,i}$, and the plausible interpolation function that satisfies these criteria and generates the cutoff time in Eq. (48)

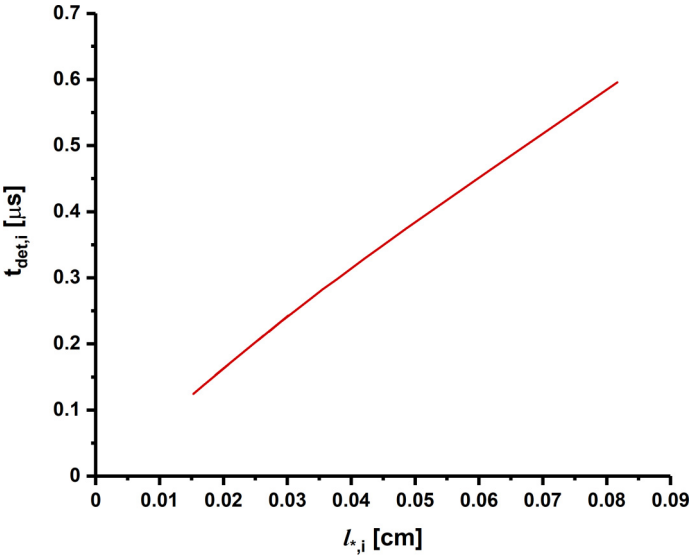

FIG. 6. The dependence of the droplet tail detachment time on its characteristic size used in the simulations in conjunction with Eq. (44).

and is shown in Fig. 6 is the following:

$$t_{\mathrm{det},i} = -1.34 \times 10^{-5}(l_{*,i})^2 + 8.34 \times 10^{-6}(l_{*,i}) + 1.70 \times 10^{-9}, \tag{49}$$

where $t_{\mathrm{det},i}$ is in μs and $l_{*,i}$ in cm, and the coefficients have the corresponding units. This function was determined through testing the required initial velocities calculated with Eq. (48), which produce trajectories corresponding to the experimental range seen in the experimental data. It should be emphasized that according to Fig. 6, $\mathrm{De} = \lambda/t_{\mathrm{det},i} \gg 1$, indeed, which corresponds to the brittle fracture regime. Note that this function satisfies the following plausible criteria: (i) it grows with the droplet size, which is physical, and (ii) it works on the scale of microseconds, i.e., once again, on physical grounds.

Drop trajectories were numerically determined using the algorithm described by this group elsewhere [13]. The predicted dependence of the number of stains on the floor to their final distance from the rear side of the target is shown in Fig. 7 in comparison with the experimental data, with the agreement being quite satisfactory.

The resultant stain area on the floor was measured experimentally and predicted following the procedure of [14], which employs the calculated impact angle of blood drops on the floor, α_i [42], and the drop spread factor for normal impact, ξ_i. Namely, a blood drop impinging onto a horizontal surface shown in Fig. 8 reveals the longest size of the drop stain $\Delta X_i = (\xi_i l_{*,i})/\sin\alpha_i$, where $\xi_i = 0.61(\mathrm{We}_i/\mathrm{Oh}_i)^{0.166}$ [43,44] with We_i and Oh_i being the final Weber and Ohnesorge numbers, respectively, based on the droplet parameters. This spread factor was first proposed by Scheller and Bousfield [43] with the validity range for viscosity of 1–300 mPa × s and the correlation coefficient of 0.963 for all of their experimental data. There is a plethora of various other spread factor correlations to choose from and they all have different ranges of validity. Some of these correlations are experimental and some others span the results of numerical simulations [45,46]. Recently, the present group showed in [47] that all those later correlations are in full agreement with the Scheller-Bousfield correlation used here.

It should be emphasized that the Ohnesorge number involves viscosity μ_{blood}, which was taken as the asymptotic value obtained in the simple shear flow, $\mu_{\mathrm{blood}} = 5$ mPa × s [27], because high shear rates accompany droplet spreading on impact [48,49]. This leads to the following expression for the

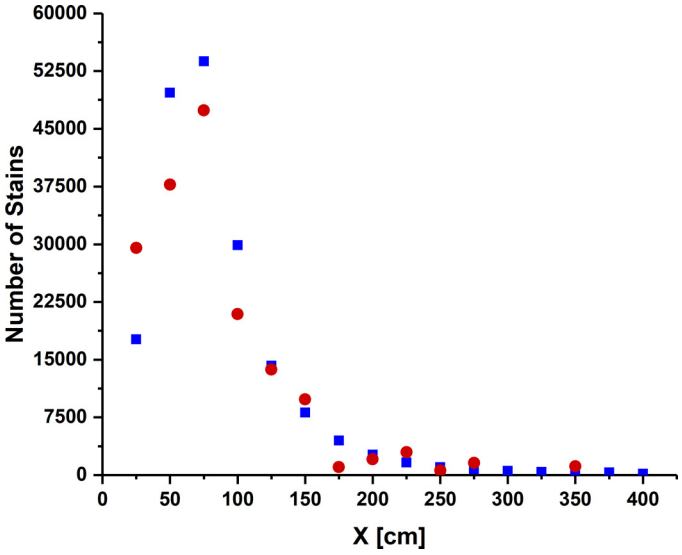

FIG. 7. The number of stains deposited on the floor vs the distance from the rear side of the target in forward blood spatter. The red circles correspond to the predicted results, and the blue squares to the experimental data. It should be emphasized that these data correspond to the combined results of five experiments as discussed in Sec. II.

stain area:

$$A_i = \frac{\pi l_{*,i}^2 {\xi_i}^2}{4 \sin \alpha_i}. \tag{50}$$

Note also that for the effect of the impact obliquity on drop spreading at the surface there are no fully reliable correlations, especially accounting for the detailed behavior of the advancing and receding contact angles (which are unknown for blood). Therefore, Eq. (50) is used to account for the effect of the impact obliquity by indirectly introducing into consideration the largest semiaxis of an elliptical stain, as is currently done in the framework of BPA [50,51].

The predicted and measured stain area are shown as a function of the distance from the rear side of the target in Fig. 9 with the agreement being fairly good. The spatial distribution in the stain area plot in Fig. 9 reveals that the initially slower, larger droplets fly further than the initially faster, smaller ones (cf. Fig. 7), which can be explained by two effects. First, the smaller drops have a lower inertia with respect to the effect of air drag and as such the trajectories of smaller drops are more affected by drag and fall shorter than those of larger drops. Second, the collective

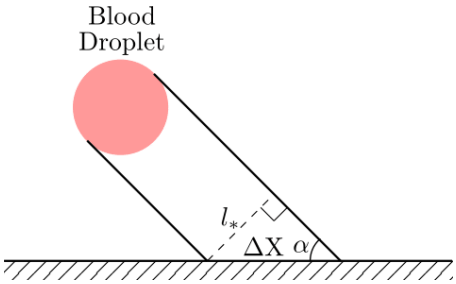

FIG. 8. Schematic of stain formation due to a blood droplet impacting onto a horizontal surface.

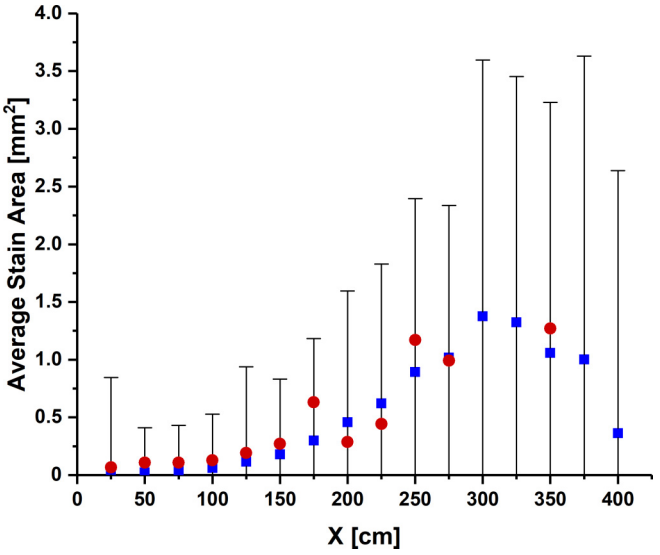

FIG. 9. The average stain area as a function of distance from the rear side of the target in forward blood spatter. The red circles depict the predictions and the blue squares are the experimental data. The error bars for the experimental data indicate the standard deviation in the stain area arising from the five experiments.

aerodynamic effect also participates in the spatial distribution in the stain area plot in Fig. 9, because the initially leading droplets create the aerodynamic wake, which reduces the drag and facilitates the flight of the subsequent larger droplets. Note that the model uses probability only to determine which part of the target is fragmented and produces detached droplets under a given bullet geometry and motion. Other than that, droplet motion is fully deterministic, and Figs. 7 and 9 represent the fully deterministic predictions. This is, essentially, similar to how detached droplets are generated, travel, and are deposited in reality.

It should be emphasized that the parameters in such experiments are very difficult to control, which results in the large standard deviations (for example, cf. Figs. 6–8 in [13]). These standard deviations do not follow a Gaussian distribution, first of all because area is an inevitably positive quantity. Also, it should be emphasized that all the outlier stain areas were included. It seems nearly impossible to create perfectly repeatable experiments because things that are seemingly minute, such as the gunpowder in the cartridge, easily change the muzzle velocity of the bullet. Or, for instance, the grain (the mass of the projectile) can be different even for the same bullet type, which is something entirely dictated by the manufacturer and would completely change the inertia of the impacting projectile. These parameters are out of the control of the police shooters conducting these experiments. Blood properties can also vary from sample to sample, which further compromises reproducibility and increases error bars, as in Fig. 9.

The offset stain area in the numerical results as compared to the experimental data may be attributed to the physical considerations under which Eq. (50) was determined. For instance, the numerical calculations neglect the evaporation of the drops during flight. Moreover, the effect of hematocrit on surface tension is unknown, even though it is plausible that it does have an effect because the surface tension of water is higher than that of blood. The addition of whey protein isolate, for instance, is known to reduce the surface tension along with temperature [52]. It should be emphasized that the most commonly used spread factor correlations are empirical and valid only for the flow regimes that they were experimentally tested on. As such, it is nearly impossible to really prove that one correlation is better or more appropriate than the other unless the correlation is tested and found for each possible deposition scenario. Note also that using the dependence of the

blood viscosity on temperature and hematocrit from [49] and of the surface temperature of blood on temperature from [53], it was found that the theoretical predictions of the dependence of the average stain area on distance (cf. Fig. 9) change insignificantly between the two limiting cases of the room and body temperature. Accordingly, the effect of drop cooling during flight on the results is insignificant.

It should be emphasized that the experimental data were collected by adding the values found in five experiments and that the number of stains in Fig. 7 was predicted accordingly, whereas the stain area in Fig. 9 was averaged. An artificial discretization of the experimental and theoretical results, as indicated in Fig. 4, can contain some stains resulting from a certain bin into a strip with the other stains, thus creating the resulting fluctuations, as for example those seen in the theoretical predictions in Fig. 9 at $x = 175$ and 250 cm.

V. CONCLUSION

This work describes a theoretical model of forward blood spatter due to a gunshot. The model is based on the approach previously applied to the problems of terminal ballistics in the framework of percolation theory. In addition, the present model incorporates the effect of the viscoelasticity of blood on droplet detachment from the target and the collective aerodynamic interaction of droplets flying through air. The theoretical predictions are corroborated versus the experimental data acquired in the present work from gunshots of a 9 mm full metal jacket bullet shot by a Glock model 19 into a cavity filled with human blood. The comparison of the predicted and measured number of blood stains found at certain distances from the rear side of the target along the bullet path revealed good agreement. The comparison of the predicted spatial distribution of the average stain area revealed a reasonable agreement. It should be emphasized, however, that the experimental results are preliminary, and in order to fully validate the proposed model, more varied experiments should be conducted in the future.

The present model predicted the following three outcomes of the forward blood spatter resulting from a gunshot: (i) the distances from the target at which blood stains appear, (ii) the distribution of the number of stains, and (iii) the distribution of the stain area. These predictions are produced in the framework of a unified approach, based on physical principles, i.e., the chaotic disintegration of blood described through percolation theory, the viscoelasticity of blood, the velocity field, the individual droplet flight affected by the gravity force, and air drag and the collective effect, which stems from the aerodynamic droplet-droplet interaction. These predictions are based on the same set of input parameters, and they are not trivial, e.g., the maximum of the number of stains and the deposition of the largest of the droplets. These nontrivial effects stem from the collective aerodynamic effect in which the leading drops create an aerodynamic wake, which lowers the drag on the subsequent ones, and as such, the slower and larger droplets can fly to a distance farther than the initially faster smaller droplets. Moreover, the model also predicts the droplet impact angle and its final velocity responsible for the stain area. To date, to the best of our knowledge, there is no other theoretical model capable of predicting any of these outcomes of the forward spattering of blood due to a gunshot based on sound physical principles.

ACKNOWLEDGMENTS

This work was financially supported by the U.S. National Institute of Justice (Award No. NIJ 2014-DN-BX-K036). The authors gratefully acknowledge Chief Criminalist Supervisor Kevin Winer, and interns Fabrin Fenton, KaeLyn Heikens, and Pamela Zimmerle for the experimental setup and data collection; Robert J. Smith for ensuring the safe execution of the experiments; Director Linda Netzel, who authorized the use of the indoor firing range; and the staff at the Kansas City Police Crime Laboratory for these experiments. Moreover, we thank Daniel Zamzow for experimental insight, David Baldwin for various experimental tasks, and Bill Ristenpart for fruitful discussion.

[1] D. Attinger, C. Moore, A. Donaldson, A. Jafari, and H. A. Stone, Fluid dynamics topics in bloodstain pattern analysis: Comparative review and research opportunities, Forensic Sci. Int. **231**, 375 (2013).
[2] S. Weidman, Strengthening forensic science in the United States: A path forward, Committee on Identifying the Needs of the Forensic Sciences Community, National Research Council, 2009, http://www.nap.edu/catalog/12589.html.
[3] P. L. Kirk, Affidavit Regarding State of Ohio V. Samuel Sheppard Court of Common Pleas, Criminal Branch, No. 64571, 26 April 1955.
[4] M. B. Illes, A. L. Carter, P. L. Laturnus, and A. B. Yamashita, Use of the backtrack^{TM} computer program for bloodstain pattern analysis of stains from downward-moving drops, Can. Soc. Forensic Sci. J. **38**, 213 (2005).
[5] A. L. Carter, The directional analysis of bloodstain patterns: Theory and experimental validation, Can. Soc. Forensic Sci. J. **34**, 173 (2001).
[6] R. Kanable, BackTrack going forward, Law Enforc. Technol. **33**, 40 (2006).
[7] A. L. Carter, J. Forsythe-Erman, V. Hawkes, M. Illes, P. Laturnus, G. Lefebvre, C. Stewart, and B. Yamashita, Validation of the BackTrack suite of programs for bloodstain pattern analysis, J. Forensic Identif. **56**, 242 (2006).
[8] A. L. Carter, M. Illes, K. Maloney, A. B. Yamashita, B. Allen, B. Brown, L. Davidson, G. Ellis, J. Gallant, A. Gradkowski, J. Hignell, S. Jory, P. L. Laturnus, C. C. Moore, R. Pembroke, A. Richard, R. Spenard, and C. Stewart, Further validation of the BackTrack^{TM} computer program for bloodstain pattern analysis-Precision and accuracy, Int. Assoc. Bloodstain Pattern Anal. News **21**, 15 (2005).
[9] W. F. Rowe, Errors in the determination of the point of origin of bloodstains, Forensic Sci. Int. **161**, 47 (2006).
[10] K. G. de Bruin, R. D. Stoel, and J. C. M. Limborgh, Improving the point of origin determination in bloodstain pattern analysis, J. Forensic Sci. **56**, 1476 (2011).
[11] N. Behrooz, Bloodstain pattern analysis for determination of point of origin, B.S. thesis, University of Toronto (2009).
[12] N. Laan, K. G. de Bruin, D. Slenter, J. Wilhelm, M. Jermy, and D. Bonn, Bloodstain pattern analysis: Implementation of a fluid dynamic model for position determination of victims, Sci. Rep. **5**, 11461 (2015).
[13] P. M. Comiskey, A. L. Yarin, S. Kim, and D. Attinger, Prediction of blood back spatter from a gunshot in bloodstain pattern analysis, Phys. Rev. Fluids **1**, 043201 (2016).
[14] P. M. Comiskey, A. L. Yarin, and D. Attinger, Hydrodynamics of back spatter by blunt bullet gunshot with a link to bloodstain pattern analysis, Phys. Rev. Fluids **2**, 073906 (2017).
[15] P. M. Comiskey, A. L. Yarin, and D. Attinger, High-speed video analysis of forward and backward spattered blood droplets, Forensic Sci. Int. **276**, 134 (2017).
[16] A. L. Yarin, I. V. Roisman, and C. Tropea, *Collision Phenomena in Liquids and Solids* (Cambridge University Press, Cambridge, 2017).
[17] L. Qi, J. Luo, J. Zhou, X. Hou, and H. Li, Prediction and measurements of deflected trajectory and temperature history of uniform metal droplets in microstructures fabrication, Int. J. Adv. Manuf. Technol. **55**, 997 (2011).
[18] P. L. Davidson, M. C. Taylor, S. J. Wilson, K. A. J. Walsh, and J. A. Kieser, Physical components of soft-tissue ballistic wounding and their involvement in the generation of blood backspatter, J. Forensic Sci. **57**, 1339 (2012).
[19] A. L. Yarin, *Free Liquid Jets and Films: Hydrodynamics and Rheology* (Longman Scientific & Technical, Harlow, NY, 1993).
[20] A. L. Yarin, I. V. Roisman, K. Weber, and V. Hohler, Model for ballistic fragmentation and behind-armor debris, Int. J. Impact Eng. **24**, 171 (2000).
[21] M. Kornfeld, *Elasticity and Strength of Liquids* (GITTL, Moscow, 1951).
[22] H. Kolsky and D. Rader, Stress waves and fracture, in *Fracture*, edited by H. Liebowitz (Academic, New York, 1969), Vol. 1.
[23] G. Cherepanov, *Mechanics of Brittle Fracture* (McGraw-Hill, New York, 1979).
[24] I. A. Dukhovskiĭ, P. I. Kovalev, and A. N. Rozhkov, Disintegration of polymer liquids at high-speed impact, Polymer Sci. A **46**, 31 (2004).

[25] M. T. Murzabayev and A. L. Yarin, Dynamics of sprinkler jets, Fluid Dyn. **20**, 715 (1985).
[26] R. Nigmatullin, *Dynamics of Multiphase Systems* (Hemisphere, New York, 1990), Vol. 1.
[27] A. Kolbasov, P. M. Comiskey, R. P. Sahu, S. Sinha-Ray, A. L. Yarin, B. S. Sikarwar, S. Kim, T. Z. Jubery, and D. Attinger, Blood rheology in shear and uniaxial elongation, Rheol. Acta **55**, 901 (2016).
[28] L. M. Milne-Thomson, *Theoretical Hydrodynamics*, 5th ed. (Macmillan, London, 1968).
[29] D. Staufer, Scaling theory of percolation clusters, Phys. Rep. **54**, 1 (1979).
[30] D. Staufer, *Introduction to Percolation Theory* (Taylor & Francis, London, 1985).
[31] S. Chien, R. G. King, R. Skalak, S. Usami, and A. L. Copley, Viscoelastic properties of human blood and red cell suspensions, Biorheology **12**, 341 (1975).
[32] A. L. Copley, R. G. King, S. Chien, S. Usami, R. Skalak, and C. R. Huang, Microscopic observations of viscoelasticity of human blood in steady and oscillatory shear, Biorheology **12**, 257 (1975).
[33] M. Brust, C. Schaefer, R. Doerr, L. Pan, M. Garcia, P. E. Arratia, and C. Wagner, Rheology of Human Blood Plasma: Viscoelastic Versus Newtonian Behavior, Phys. Rev. Lett. **110**, 078305 (2013).
[34] A. L. Yarin, B. Pourdeyhimi, and S. Ramakrishna. *Fundamentals and Applications of Micro- and Nanofibers* (Cambridge University Press, Cambridge, 2014).
[35] J. W. Hoyt, J. J. Taylor, and C. D. Runge, The structure of jets of water and polymer solution in air, J. Fluid Mech. **63**, 635 (1974).
[36] M. Farhat, M. Tinguely, and M. Rouvinez, *Cavitation Induced by High Speed Impact of a Solid Surface on a Liquid Jet*, American Physical Society Division of Fluid Dynamics Conference, 2009 (APS, New York, 1990).
[37] E. L. Bradley III and J. Sacerio, The velocity of ultrasound in human blood under varying physiologic parameters, J. Surg. Res. **12**, 290 (1972).
[38] Z. Rosenberg and E. Dekel. *Terminal Ballistics* (Springer, Berlin, 2012).
[39] The Edgerton Digital Collections Project, Massachusetts Institute of Technology, https://www.edgerton-digital-collections.org (accessed April 2018).
[40] Ames Laboratory Midwest Forensics Resource Center, MFRC Blood Pattern Analysis Videos, https://www.ameslab.gov/mfrc/bpa-videos (accessed April 2018).
[41] U. Windberger, A. Bartholovitsch, R. Plasenzotti, K. J. Korak, and G. Heinze, Whole blood viscosity, plasma viscosity, and erythrocyte aggregation in nine mammalian species: Reference values and comparison of data, Exp. Physiol. **88**, 431 (2003).
[42] C. Rizer, *Police Mathematics* (Thomas, Springfield, 1955).
[43] B. L. Scheller and D. W. Bousfield, Newtonian drop impact with a solid surface, AIChE J. **41**, 1357 (1995).
[44] A. L. Yarin, Drop impact dynamics: Splashing, spreading, receding, bouncing …, Annu. Rev. Fluid Mech. **38**, 159 (2006).
[45] J. Eggers, M. A. Fontelos, C. Josserand, and S. Zaleski, Drop dynamics after impact on a solid wall: Theory and simulations, Phys. Fluids **22**, 062101 (2010).
[46] G. Lagubeau, M. A. Fontelos, C. Josserand, A. Maurel, V. Pagneux, and P. Petitjeans, Spreading dynamics of drop impacts, J. Fluid Mech. **713**, 50 (2012).
[47] R. P. Sahu, S. Sett, A. L. Yarin, and B. Pourdeyhimi, Impact of aqueous suspension drops onto non-wettable membranes: Hydrodynamic focusing and penetration of nanoparticles, Colloids Surf., A **467**, 31 (2015).
[48] C. Antonini, A. Amirfazli, and M. Marengo, Drop impact and wettability: From hydrophilic to superhydrophobic surfaces, Phys. Fluids **24**, 102104 (2012).
[49] S. Kim, Y. Ma, P. Agrawal, and D. Attinger, How important is it to consider target properties and hematocrit in bloodstain pattern analysis? Forensic Sci. Int. **266**, 178 (2016).
[50] N. Laan, K. G. de Bruin, D. Bartolo, C. Josserand, and D. Bonn, Maximum diameter of impacting liquid droplets, Phys. Rev. Appl. **2**, 044018 (2014).
[51] C. D. Adam, Experimental and theoretical studies of the spreading of bloodstains on painted surfaces, Forensic Sci. Int. **229**, 66 (2013).
[52] B. Adhikari, T. Howes, A. Shrestha, and B. R. Bhandari, Effect of surface tension and viscosity on the surface stickiness of carbohydrate and protein solutions, J. Food Eng. **79**, 1136 (2007).
[53] J. Rosina, E. Kvasnák, D. Suta, H. Kolárová, J. Málek, and L. Krajcu, Temperature dependence of blood surface tension, Physiol. Res. **56**, S93 (2007).